

A New Investigation of the Cl^- – CO_3^{2-} Substitution in AFm Phases

Adel Mesbah,^{‡,§} Céline Cau-dit-Coumes,[‡] Fabien Frizon,[‡] Fabrice Leroux,^{§,¶} Johann Ravaux^{||}
and Guillaume Renaudin^{‡,¶,‡‡}

[‡]Commissariat à l'Énergie Atomique et aux énergies alternatives, CEA DEN/DTCD/SPDE,
F-30207 Bagnols sur Cèze, France

[§]Clermont Université, Université Blaise Pascal, Laboratoire des Matériaux Inorganiques,
F-63000 Clermont-Ferrand, France

[¶]CNRS, UMR 6002, F-63177 Aubière, France

^{||}Institut de Chimie Séparative de Marcoule, UMR 5257 CEA/CNRS/UM2/ENSCM, F-30207 Bagnols-sur-Cèze, France

^{‡‡}ENSCCF, Laboratoire des Matériaux Inorganiques, Clermont Université, F-63000 Clermont-Ferrand, France

Chloride to carbonate substitution in AFm phase of general formulae $[\text{Ca}_2\text{Al}(\text{OH})_6] \cdot [\text{Cl}_{1-x} \cdot (\text{CO}_3)_{x/2} \cdot (2+x/2)\text{H}_2\text{O}]$ (or $3\text{CaO} \cdot \text{Al}_2\text{O}_3 \cdot (\text{CaCl}_2)_{1-x} \cdot (\text{CaCO}_3)_x \cdot (10+x)\text{H}_2\text{O}$ written in cement notation) has been characterized by studying 12 powdered samples synthesized at 25° and at 85°C. The existence of a solid solution has been highlighted. It forms one stable rhombohedral $[\text{Ca}_2\text{Al}(\text{OH})_6] \cdot [\text{Cl}_{1-x} \cdot (\text{CO}_3)_{x/2} \cdot (2+x/2)\text{H}_2\text{O}]$ solid solution with $0.25 \leq x \leq 0.95$, isotypic with the recently described R3c chloro-carboaluminate of $[\text{Ca}_2\text{Al}(\text{OH})_6] \cdot [\text{Cl}_{0.5} \cdot (\text{CO}_3)_{0.25} \cdot 2.25\text{H}_2\text{O}]$ composition. A second metastable monoclinic $[\text{Ca}_2\text{Al}(\text{OH})_6] \cdot [\text{Cl}_{1-x} \cdot (\text{CO}_3)_{x/2} \cdot (2+x/2)\text{H}_2\text{O}]$ solid solution has also been identified in a less extended x domain. The structural relationship between these two stable and metastable chloro-carboaluminate polymorphs shows similarities with the structural transition of the Friedel's salt (from rhombohedral high-temperature-structure to monoclinic low-temperature-structure at about 35°C). The two $[\text{Ca}_2\text{Al}(\text{OH})_6] \cdot [\text{Cl}_{1-x} \cdot (\text{CO}_3)_{x/2} \cdot (2+x/2)\text{H}_2\text{O}]$ solid solutions are simultaneously present, in quite equivalent weight amounts, in samples synthesized at room temperature, whereas only the stable rhombohedral polymorph is observed for samples synthesized at 85°C. Raman spectroscopy has been successfully used to locate carbonate in the structure. The $[\text{CO}_3]$ symmetric stretching mode is observed at 1068 cm^{-1} for monocarboaluminate ($x = 1$) for carbonate directly bonded to main layer, while it is observed at 1086 cm^{-1} for both chloro-carboaluminate polymorphs, which is characteristic of interlayer carbonate.

I. Introduction

THE cement hydration process leads to precipitation of several calcium aluminate hydrates. Ettringite, the AFt phase of composition $\text{Ca}_6\text{Al}_2(\text{OH})_{12}(\text{SO}_4)_3 \cdot 26\text{H}_2\text{O}$, is the first hydrate of this family to precipitate during the early stage of hydration. In a second stage, when the sulfate concentration in the cement paste solution decreases due to ettringite precipitation, monosulfoaluminate, which is the sulfate AFm phase $\text{Ca}_2\text{Al}(\text{OH})_6 \cdot (\text{SO}_4)_{1/2} \cdot 3\text{H}_2\text{O}$, becomes stable at the expense of ettringite. AFm phases, of general formulae $\text{Ca}_2\text{Al}(\text{OH})_6 \cdot$

$X_z \cdot n\text{H}_2\text{O}$ where X_z is either one singly charged anions or half a doubly charged anion, depending on the cement paste anionic composition are observed. They belong to the lamellar double hydroxide family and are composed of positively charged main layer $[\text{Ca}_2\text{Al}(\text{OH})_6]^+$ and negatively charged interlayer $[X_z^- \cdot n\text{H}_2\text{O}]$. The main anions encountered in AFm chemistry are carbonate CO_3^{2-} ,^{1,2} sulfate SO_4^{2-} ,³ and chloride Cl^- .^{4–6} Nevertheless, numerous others anions can insert the AFm interlayer region: nitrate NO_3^- ,^{7,8} bromide Br^- ,⁹ iodide I^- ,^{10,11} chromate CrO_4^{2-} ,^{12,13} ... The chemistry of AFm phases has been widely studied.^{14–17} Owing to their anionic exchange capacity,¹⁸ these compounds may be considered as good candidates to bind anionic radionuclides present in nuclear wastes such as chloride and carbonate (³⁶Cl and ¹⁴C). The present work aims at investigating the possibility to trap simultaneously these two anions by considering the occurrence of a solid solution between singly charged chloride and doubly charged carbonate anions of general formulae $[\text{Ca}_2\text{Al}(\text{OH})_6] \cdot [\text{Cl}_{1-x} \cdot (\text{CO}_3)_{x/2} \cdot 2.25\text{H}_2\text{O}]$. The crystallographic structure of the two end-members is well known; i.e. the monocarboaluminate phase (with $x = 1$: $[\text{Ca}_2\text{Al}(\text{OH})_6] \cdot [(\text{CO}_3)_{1/2} \cdot 2.5\text{H}_2\text{O}]$ or $\text{Ca}_3\text{Al}_2\text{O}_6 \cdot \text{CaCO}_3 \cdot 11\text{H}_2\text{O}$ in cement notation) and Friedel's salt (with $x = 0$: $[\text{Ca}_2\text{Al}(\text{OH})_6] \cdot [\text{Cl} \cdot 2\text{H}_2\text{O}]$ or $\text{Ca}_3\text{Al}_2\text{O}_6 \cdot \text{CaCl}_2 \cdot 10\text{H}_2\text{O}$ in cement notation). The structure of Friedel's salt has been investigated by Terzis *et al.*⁶ with the monoclinic $C2/c$ symmetry, and revisited by Rapin and colleagues.^{4,5} The structure of monocarboaluminate has been solved and refined from X-ray single-crystal diffraction. Two modifications have been observed: an ordered arrangement with the triclinic $P1$ symmetry,¹ and a disordered arrangement with the triclinic $P\bar{1}$ symmetry.² AFm compounds containing simultaneously the chloride and carbonate anions have been reported in the literature. The first one, called hydrocalumite, is a natural mineral. Its structure has been solved by Sacerdoti and Passaglia¹⁹ in the monoclinic $P2/c$ space group with the general formula $[\text{Ca}_2\text{Al}(\text{OH})_6] \cdot [\text{Cl}_{1/2} \cdot (\text{CO}_3)_{1/4} \cdot 2.4\text{H}_2\text{O}]$. Chloride and carbonate anions are ordered in independent crystallographic positions at the center of the interlayer region. The authors indicate that the structure can be described in the $C2/c$ symmetry with a half- b parameter and a statistical distribution of chloride and carbonate anions in a unique crystallographic position. The average $C2/c$ description of hydrocalumite is isotypic with the Friedel's salt low-temperature (LT)-structure.^{4,6} A synthesized chloro-carboaluminate compound with a similar composition has been recently described in the rhombohedral $R3c$ symmetry.²⁰ This rhombohedral chloro-carboaluminate hydrate is isotypic with the Friedel's salt high-temperature (HT)-structure.⁵ Chloride and

P. Brown—contributing editor

Manuscript No. 28318. Received July 16, 2010; approved November 3, 2010.

[†]Author to whom correspondence should be addressed. e-mail: guillaume.renaudin@ensccf.fr

carbonate anions are located in the same crystallographic position with a statistical distribution. Crystallographic details (lattice parameters and symmetries) for AFm phases containing chloride and carbonate anions are available in Table I.

Very recently, an extensive solid solution was found between Friedel's salt and monocarboaluminate²¹ with miscibility gap below 0.1 Cl/(Cl+1/2CO₃) in rather good agreement with previous results (<0.1 Cl according to Pöllman²² and ≤0.09 Cl according to Hobles²³).

The occurrence and description of this [Ca₂Al(OH)₆]·[Cl_{1-x}·(CO₃)_{x/2}] solid solutions are examined in detail in this paper by considering the crystallographic structure of the precipitated hydrates. Rietveld analyses of X-ray powder patterns were systematically performed in order to take into account not only the interlayer distance but also the actual symmetry of the phases, i.e. the potential presence of polymorphism and formation of solid solutions. Two series of samples were prepared by precipitation in solution at 25° and 85°C with different chloride/

carbonate ratios. The resulting powders were characterized by powder X-ray diffraction (PXRD) using the Rietveld method; the chemical compositions of the hydrates were determined by scanning electron microscopy (SEM) analyses. Raman spectroscopy was efficiently used to investigate the carbonate environment in the different phases, as well as to characterize the hydrogen bond network in the interlayer space. ²⁷Al MAS NMR spectroscopy allowed discriminating the different AFm phases.

II. Experimental Section

(1) Synthesis

Powder samples with nominal composition [Ca₂Al(OH)₆]·[Cl_{1-x}·(CO₃)_{x/2}·(2+x/2)H₂O] were synthesized in aqueous solution. The starting powders Ca₃Al₂O₆, CaCl₂·2H₂O (Aldrich) and CaCO₃ (Aldrich, Lyon, France) were mixed in demineralized and decarbonated water to reach a water/solid mass ratio of

Table I. Crystallographic Data of Selected AFm Phases Taken From the Literature. Standard Deviations for Lattice Parameters and Unit Cell Volume are Indicated in Parentheses

| Compound name Chemical composition Symmetry, space group Z (motif: [Ca ₂ Al(OH) ₆]·[X _z ·nH ₂ O]). | Lattice parameters Unit cell volume | Reference |
|--|---|---------------------------------------|
| Monocarboaluminate (ordered phase) O-3CaO·Al ₂ O ₃ ·CaCO ₃ ·11H ₂ O Triclinic, <i>P</i> 1 2 | <i>a</i> = 5.775 (1) Å <i>b</i> = 8.469 (1) Å <i>c</i> = 9.923 (3) Å <i>α</i> = 64.77 (2)° <i>β</i> = 82.75 (2)° <i>γ</i> = 81.43 (2)° <i>V</i> = 433.0 (2) Å ³ | François <i>et al.</i> ¹ |
| Monocarboaluminate (disordered phase) D-3CaO·Al ₂ O ₃ ·CaCO ₃ ·11H ₂ O Triclinic, <i>P</i> 1̄ 2 | <i>a</i> = 5.7422 (4) Å <i>b</i> = 5.7444 (4) Å <i>c</i> = 15.091 (3) Å <i>α</i> = 92.29 (1)° <i>β</i> = 87.45 (1)° <i>γ</i> = 119.547 (7)° <i>V</i> = 432.5 (1) Å ³ | Renaudin <i>et al.</i> ² |
| Friedel's salt (low-temperature phase) LT-3CaO·Al ₂ O ₃ ·CaCl ₂ ·10H ₂ O Monoclinic, <i>C</i> 2/ <i>c</i> 4 | <i>a</i> = 9.960 (4) Å <i>b</i> = 5.7320 (2) Å <i>c</i> = 16.268 (7) Å <i>β</i> = 104.471 (2)° <i>V</i> = 898.97 (1) | Rapin <i>et al.</i> ⁴ |
| Friedel's salt (high-temperature phase) HT-3CaO·Al ₂ O ₃ ·CaCl ₂ ·10H ₂ O Rhombohedral, <i>R</i> 3̄ <i>c</i> 6 | <i>a</i> = 5.744 (2) Å <i>c</i> = 46.89 (3) Å <i>V</i> = 1339.8 (7) Å ³ | Rapin <i>et al.</i> ⁴ |
| Hydrocalumite 3CaO·Al ₂ O ₃ ·1/2CaCl ₂ ·1/2CaCO ₃ ·10.8H ₂ O Monoclinic, <i>P</i> 2/ <i>c</i> 8 | <i>a</i> = 10.020(1) Å <i>b</i> = 11.501(1) Å <i>c</i> = 16.286(3) Å <i>β</i> = 104.22(1)° <i>V</i> = 1819.29 (2) | Sacerdoti and Passaglia ¹⁹ |
| Hydrocalumite (average description) 3CaO·Al ₂ O ₃ ·1/2CaCl ₂ ·1/2CaCO ₃ ·10.8H ₂ O Monoclinic <i>C</i> 2/ <i>c</i> 4 | <i>a</i> = 10.020(1) Å <i>b</i> = 5.751(1) Å <i>c</i> = 16.286(3) Å <i>β</i> = 104.22(1)° <i>V</i> = 909.64 (1) Å ³ | Sacerdoti and Passaglia ¹⁹ |
| Chloro-carboaluminate 3CaO·Al ₂ O ₃ ·1/2CaCl ₂ ·1/2CaCO ₃ ·10.5H ₂ O Rhombohedral <i>R</i> 3̄ <i>c</i> 6 | <i>a</i> = 5.740 (1) Å <i>c</i> = 46.74 (1) Å <i>V</i> = 1333.7 (2) Å ³ | Mesbah <i>et al.</i> ²⁰ |

50. All the suspensions were stored under nitrogen and continuous stirring. Two series of samples were prepared: one kept at room temperature for 1 month in closed polypropylene bottles (eight samples with $x = 1.00, 0.95, 0.90, 0.85, 0.80, 0.75, 0.50,$ and 0.25), and a second kept at 85°C for 3 weeks in closed Teflon reactors (four samples with $x = 1.00, 0.75, 0.5,$ and 0.25). Depending on the temperature (respectively 25° and 85°C) used for synthesis, samples were respectively designated as AFm-[Cl $_{1-x}$ ·(CO $_3$) $_{x/2}$]- 25°C and AFm-[Cl $_{1-x}$ ·(CO $_3$) $_{x/2}$]- 85°C . Twelve samples are studied in the paper: AFm-[(CO $_3$) $_{0.500}$]- 25°C , AFm-[Cl $_{0.05}$ ·(CO $_3$) $_{0.475}$]- 25°C , AFm-[Cl $_{0.10}$ ·(CO $_3$) $_{0.450}$]- 25°C , AFm-[Cl $_{0.15}$ ·(CO $_3$) $_{0.425}$]- 25°C , AFm-[Cl $_{0.20}$ ·(CO $_3$) $_{0.400}$]- 25°C , AFm-[Cl $_{0.25}$ ·(CO $_3$) $_{0.375}$]- 25°C , AFm-[Cl $_{0.50}$ ·(CO $_3$) $_{0.250}$]- 25°C , AFm-[Cl $_{0.75}$ ·(CO $_3$) $_{0.125}$]- 25°C , AFm-[(CO $_3$) $_{0.500}$]- 85°C , AFm-[Cl $_{0.25}$ ·(CO $_3$) $_{0.375}$]- 85°C , AFm-[Cl $_{0.50}$ ·(CO $_3$) $_{0.250}$]- 85°C , and AFm-[Cl $_{0.75}$ ·(CO $_3$) $_{0.125}$]- 85°C .

At the end of the experiments, the suspensions were centrifuged and rinsed twice in demineralized and decarbonated water before performing a third centrifugation with isopropanol. The precipitates were subsequently dried in a dessicator, under slight vacuum, over potassium acetate ($\approx 20\%$ r.h.) at room temperature.

(2) PXRD

PXRD patterns were recorded on an X'Pert Pro Philips diffractometer (Almelo, the Netherlands), with θ - θ geometry, equipped with a solid detector X-Celerator, a graphite back-end monochromator, and using $\text{CuK}\alpha$ radiation ($\lambda = 1.54184 \text{ \AA}$). PXRD patterns were recorded at room temperature in the interval $3^\circ < 2\theta < 120^\circ$, with a step size $\Delta 2\theta = 0.0167^\circ$ and a total counting time of 3 h. Ten weight percent of pure silicon powder was added in all samples and intimately mixed before the PXRD acquisition in order to improve the Rietveld refinement procedure and allow: (1) the precise refinement of the zero shift, (2) the checking of the quantitative Rietveld analysis results, and (3) the extraction of the instrumental resolution function directly from each measured powder pattern in order to improve the peak shape modeling. All powder patterns were treated by the Rietveld method using the Thomson-Cox-Hastings Pseudo Voigt convoluted with an axial divergence asymmetry function²⁴ with the Fullprof_Suite program.²⁵ During the refinement procedure, the following parameters were allowed to vary: zero shift, scale factors, preferred orientation, asymmetry parameters, lattice parameters, global thermal displacement for each phase, site occupancies (when justified), and intrinsic microstructure parameters to extract crystal size effect. The Brindley corrections were not applied because mD was below 0.01 (m is the linear absorption coefficient and D the linear particle size). Each refinement led to good conventional Rietveld agreement factors. PXRD patterns recorded for both series are shown in Fig. 1. Rietveld plots for AFm-[Cl $_{0.25}$ ·(CO $_3$) $_{0.375}$]- 25°C and AFm-[Cl $_{0.25}$ ·(CO $_3$) $_{0.375}$]- 85°C samples are shown, as examples, in Fig. 2.

(3) Raman Spectroscopy

Micro-Raman spectra were recorded at room temperature in the back scattering geometry, using a Jobin-Yvon T64000 device (Lille, France). The spectral resolution, about 1 cm^{-1} , was obtained with an excitation source at 514.5 nm (argon ion laser line, Spectra Physics 2017, Villebon sur Yvette, France). The Raman detector was a charge coupled device multichannel detector cooled down at 140 K by liquid nitrogen. The laser beam was focused onto the sample through an Olympus confocal microscope (Rungis, France) with $\times 100$ magnification. The laser spot was about $1 \mu\text{m}^2$. The measured power at the sample level was kept low ($< 15 \text{ mW}$) in order to avoid any damage of the material. The Raman scattered light was collected with a microscope objective at 360° from the excitation and filtered with an holographic Notch filter before being dispersed by a single grating (1800 grooves/mm). Spectra were recorded (four scans of 120 s) in the frequencies ranges of 200 – 1800 and 2800 – 3900 cm^{-1} in order to investigate, respectively, the Raman active vibration modes of carbonate anion and the hydrogen bond net-

work due to O–H stretching. Spectra were analyzed by a profile fitting procedure using a Lorentzian function.

(4) SEM

SEM analyses were performed with a field-emission gun electron microscope (FEI QUANTA 200 ESEM FEG model, Eindhoven, the Netherlands) coupled with a Bruker SDD 5010 energy-dispersive spectrometer (Berlin, Germany). As the compounds to be analyzed may be damaged under the electron beam, the beam current was lowered by using a $30 \mu\text{m}$ aperture, the acceleration voltage was maintained at 15 kV , and the acquisition time was limited to 30 s . The elemental quantification was performed using external standards: Ca (CaSiO $_4$), Al (NaAlSi $_3$ O $_8$), Cl (PbCl $_2$), and O (NaAlSi $_3$ O $_8$), respectively.

The samples were prepared by dispersion in ethanol and deposited on a carbon holder, and fully carbon coating. The particle sizes ranged between 0.5 and $20 \mu\text{m}$. The analyses were performed on crystals that were strictly isolated from the others.

At least 50 measurements were performed on one sample, each analysis being recorded on a different crystal. A statistical treatment of the analyses population led to reject the values that were out of the confidence interval. The mean value and the standard deviations were determined and reported for each sample in Table II. The carbonate amount in the $[\text{Ca}_2\text{Al}(\text{OH})_6] \cdot [\text{Cl}_{1-x}(\text{CO}_3)_{x/2} \cdot (2+x/2)\text{H}_2\text{O}]$ phases was calculated by assuming electroneutrality.

(5) ^{27}Al MAS NMR Spectroscopy

High-resolution ^{27}Al MAS NMR spectra were collected on a Bruker 300 instrument (Wissenbourg, France) operating at 7.04 T , the Larmor frequencies being equal to 78.20 MHz . 4-mm -diameter zirconia rotors were spun at 10 kHz during the MAS conditions; therefore, only the central transition ($+1/2, -1/2$) was recorded using a single-pulse experiment. The quadrupolar nature of ^{27}Al ($5/2$) nucleus required that the flip angle should satisfy the condition $(I + 1/2)\omega_{\text{RF}}t_p \leq \pi/6$ where ω_{RF} (rad/s) is the Larmor frequency of the quadrupolar ^{27}Al nucleus and t_p (s) the pulse time. Small pulse angles of about 10° corresponding to 0.8 – 1.2 ms pulses were used in the MAS sequence. This was associated to a recycling time of 2 s . Calibration was adjusted with the resonance line of AlCl $_3$ at 0 ppm . A collection of 2000 transients to obtain a proper signal to noise response was necessary. Single-pulse experiment is quantitative and therefore the relative nuclei site population was accessible. However for noninteger quadrupolar nuclei, the central transition is not perturbed by the first-order quadrupolar interaction, while the second order is known to broaden the resonance line as well as to shift its position from the isotropic chemical shift. The fast MAS spectrum of the central ($+1/2, -1/2$) is then shifted from the center of gravity by the second-order quadrupolar interaction $\delta_{\text{QS}(+1/2,-1/2)}^{(2)} = -\frac{3C_Q}{40\omega_0^2} \left[\frac{I(I+1)-3/4}{I^2(2-1)^2} \right] \left(1 + \frac{\eta^2}{3} \right)$ where C_Q is the quadrupolar coupling ($C_Q = e^2qQ/h$, e,q is the electric field gradient and $e.Q$ is the quadrupolar moment of values of 0.15 – 10^{28} Q/m^2 for ^{27}Al nuclei), and η is the asymmetry parameter. The isotropic chemical shift position and the quadrupolar frequency ν_Q (responsible for $\delta_{\text{QS}(+1/2,-1/2)}^{(2)}$) may be obtained by measurements either at different magnetic fields²⁶ or of the central and of the sideband patterns of the satellite transitions.²⁷ The shift of the central band is then given by $\delta_{\text{QS}(+1/2,-1)}^{(2)} = -\frac{\nu_Q^2}{30\omega_0^2} [I(I+1) - 3/4] 10^6$, which can be further calculated for ^{27}Al by $\delta_{\text{QS}(+1/2,-1/2)}^{(2)} = -\frac{8\nu_Q^2}{30\omega_0^2} 10^6$. For ^{27}Al , ν_Q ranges from 0.15 to 0.35 for Al(VI), from 0.4 to 0.5 for Al(V), and from 0.2 to 0.5 for Al(IV).^{28,29}

In the following, the chemical shifts were neither corrected for second-order quadrupolar effects nor reported as isotropic values. The maximum intensity positions were comparatively discussed for the two series.

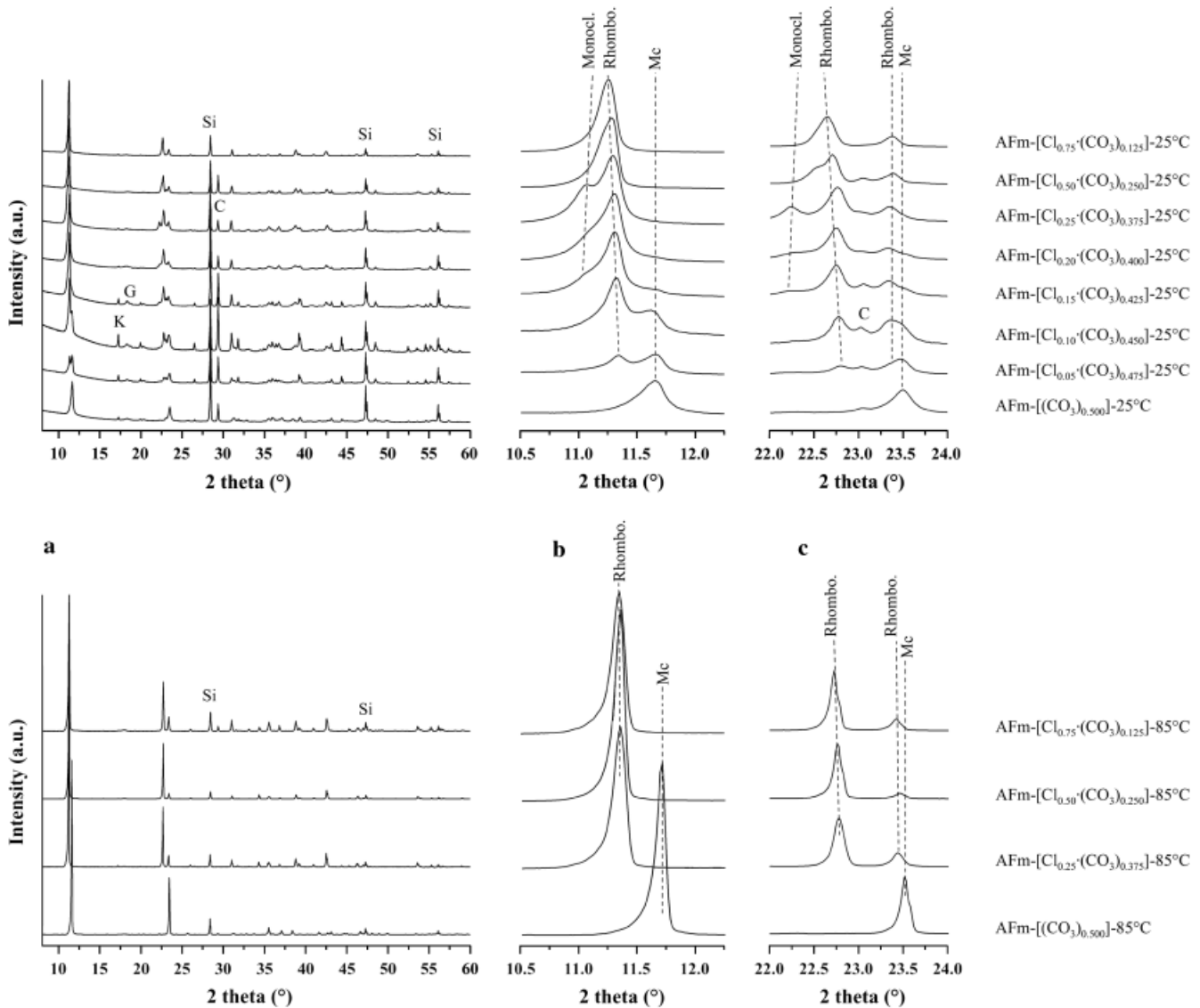


Fig. 1. PXRD patterns recorded for the eight samples belonging to the AFm-[Cl_{1-x}·(CO₃)_{x/2}]-25°C series (top) and the four samples belonging to the AFm-[Cl_{1-x}·(CO₃)_{x/2}]-85°C series (bottom): large 2θ scale from 8° to 60° (a), zoom showing the first (00l) diffraction peaks from 10.5° to 12° (b), and zoom showing the second-order (00l) diffraction peaks from 22° to 24° (c). AFm phases are indicated by Mc (monocarboaluminate), Rhombo. (the rhombohedral polymorph of chloro-carboaluminate) and Monocl. (the monoclinic polymorph of chloro-carboaluminate). Impurities are indicated by C (calcite), K (katoite), and G (gibbsite), and Si relates the internal silicon standard.

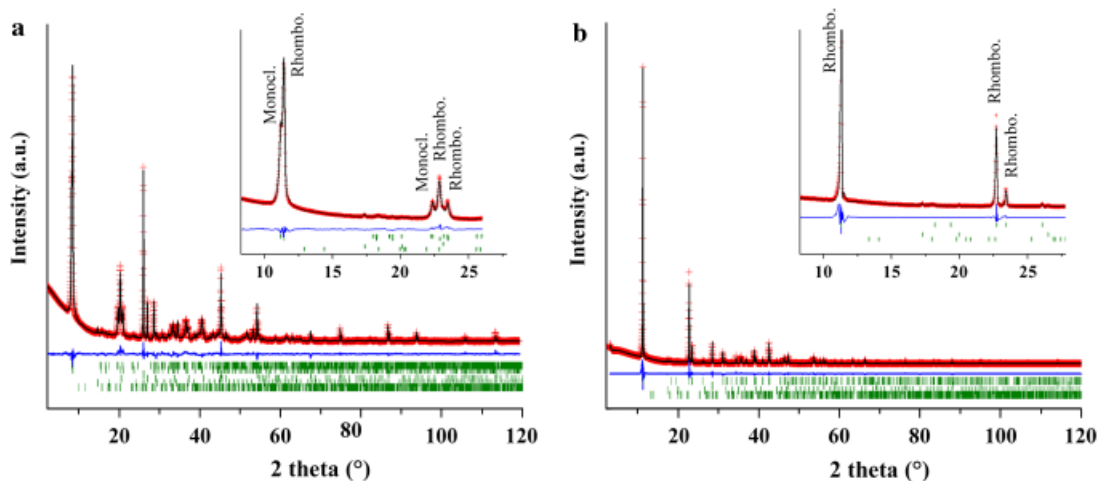


Fig. 2. Rietveld plot: observed patterns (red crosses), calculated patterns (black curves), and difference lines (blue curves) for a: AFm-[Cl_{0.25}·(CO₃)_{0.375}]-25°C and b: AFm-[Cl_{0.25}·(CO₃)_{0.375}]-85°C samples. Rhombo and Monocl refer respectively to diffraction peaks from rhombohedral and monoclinic chloro-carboaluminate polymorphs.

Table II. Rietveld Quantitative Results for the Three AFm Phases Present in Samples from Both AFm-[Cl_{1-x}·(CO₃)_{x/2}]-25°C and AFm-[Cl_{1-x}·(CO₃)_{x/2}]-85°C Series

| Sample | $x_{nom.}^\dagger$ | $x_{exp.}^\ddagger$ | $x_{ref.}^\ddagger$ | Chloro-carboaluminate | | Monocarboaluminate |
|--|--------------------|---------------------|---------------------|-----------------------|------------|--------------------|
| | | | | R $\bar{3}c$ (wt%) | C2/c (wt%) | P1 (wt%) |
| <i>AFm-[Cl_{1-x}·(CO₃)_{x/2}]-25°C series</i> | | | | | | |
| AFm-[Cl _{0.75} ·(CO ₃) _{0.125}]-25°C | 0.25 | 0.29 (4) | 0.20 (4) | 100 (-) | — | — |
| AFm-[Cl _{0.50} ·(CO ₃) _{0.250}]-25°C | 0.50 | 0.38 (4) | 0.50 (4) | 56 (2) | 44 (2) | — |
| AFm-[Cl _{0.25} ·(CO ₃) _{0.375}]-25°C | 0.75 | 0.75 (1) | 0.76 (4) | 54 (2) | 46 (2) | — |
| AFm-[Cl _{0.20} ·(CO ₃) _{0.400}]-25°C | 0.80 | 0.79 (1) | 0.80 (4) | 51 (4) | 48 (4) | 1 (4) |
| AFm-[Cl _{0.15} ·(CO ₃) _{0.425}]-25°C | 0.85 | 0.84 (2) | 0.82 (4) | 60 (4) | 35 (4) | 5 (4) |
| AFm-[Cl _{0.10} ·(CO ₃) _{0.450}]-25°C | 0.90 | 0.90 (2) | 0.92 (4) | 52 (4) | 8 (4) | 40 (4) |
| AFm-[Cl _{0.05} ·(CO ₃) _{0.475}]-25°C | 0.95 | 0.95 (1) | 0.96 (4) | 30 (4) | 4 (4) | 66 (4) |
| AFm-[(CO ₃) _{0.500}]-25°C | 1.00 | — | — | — | — | 100 (-) |
| <i>AFm-[Cl_{1-x}·(CO₃)_{x/2}]-85°C series</i> | | | | | | |
| AFm-[Cl _{0.75} ·(CO ₃) _{0.125}]-85°C | 0.25 | 0.22 (4) | 0.20 (4) | 100 (-) | — | — |
| AFm-[Cl _{0.50} ·(CO ₃) _{0.250}]-85°C | 0.50 | 0.51 (4) | 0.54 (4) | 100 (-) | — | — |
| AFm-[Cl _{0.25} ·(CO ₃) _{0.375}]-85°C | 0.75 | 0.73 (3) | 0.78 (4) | 100 (-) | — | — |
| AFm-[(CO ₃) _{0.500}]-85°C | 1.00 | — | — | — | — | 100 (-) |

[†] $x_{nom.}$, $x_{exp.}$, and $x_{ref.}$ represent respectively the x targeted nominal values, the x calculated values from the SEM analyses of AFm-[Cl_{1-x}·(CO₃)_{x/2}] samples, and the refined x values from Rietveld analyses for the chloro-carboaluminate [Ca₂Al(OH)₆]·[Cl_{1-x}·(CO₃)_{x/2}·(2+x/2)H₂O] rhombohedral polymorph.

III. Results

(1) Rietveld Analyses

(A) *Mineralogical Composition of Samples Belonging to the AFm-[Cl_{1-x}·(CO₃)_{x/2}]-25°C series:* The following AFm phases were identified by XRD:

(1) One triclinic phase corresponding to monocarboaluminate (Ca₄Al₂(OH)₁₂CO₃·5H₂O) was observed at high x values ($x > 0.80$). The ordered P1 structural model¹ was considered here.

(2) Two chloro-carboaluminate phases due to polymorphism were observed. As described in our previous structural study on chloro-carboaluminate,²⁰ occurrence of rhombohedral and monoclinic polymorphs was observed. Rhombohedral and respectively monoclinic chloro-carboaluminate occurred for x with the range [0.25; 0.95] and respectively [0.50; 0.95].

Monocarboaluminate predominated for $x \geq 0.95$, while chloro-carboaluminate was the main species at lower x values. All the samples from the AFm-[Cl_{1-x}·(CO₃)_{x/2}]-25°C series with $0.50 \leq x \leq 0.95$ could therefore be roughly described by a two-phase mixture composed of the rhombohedral polymorph of chloro-carboaluminate and either the monoclinic polymorph of chloro-carboaluminate or monocarboaluminate. Mono-

carboaluminate was replaced by the monoclinic chloro-carboaluminate polymorph when the x nominal value decreases from 1.00 to 0.80 (Fig. 3). Some impurities were also observed: calcite, katoite (C₃AH₆), and poorly crystalline gibbsite and/or bayerite (AH₃). All these impurities (as well as the added pure silicon standard) were taken into account in the Rietveld refinement procedures. Weight amounts of impurities were less than a few percent. Refined weight amounts of the three AFm phases for both series are indicated in Table II, and their variations versus the x nominal value are shown in Fig. 3 for the AFm-[Cl_{1-x}·(CO₃)_{x/2}]-25°C series (impurities were excluded for better clarity). The weight amount of the rhombohedral chloro-carboaluminate polymorph fluctuated around 55% for $0.50 \leq x \leq 0.90$, and reached 100% for $x = 0.25$. The residual 45 wt% for $0.50 \leq x \leq 0.95$ were composed of monocarboaluminate at high x values ($x \geq 0.90$) or the monoclinic chloro-carboaluminate polymorph at lower x values ($x \leq 0.85$). The monocarboaluminate weight amount decreased deeply when chloride was introduced (66 wt% for $x = 0.95$, 40 wt% for $x = 0.90$, and 5 wt% only for $x = 0.85$), which was compensated by the formation of monoclinic chloro-carboaluminate (4 wt% for $x = 0.95$, 8 wt% for $x = 0.90$, and 35 wt% only for $x = 0.85$). It appears from this quantitative phase analysis that the monoclinic chloro-carboaluminate polymorph interrelates with the carbonate-rich side of the assumed [Ca₂Al(OH)₆]·[Cl_{1-x}·(CO₃)_{x/2}·(2+x/2)H₂O] solid solution (i.e., interrelates with triclinic monocarboaluminate) whereas the rhombohedral polymorph interrelates with the chloride-rich side (i.e., interrelates to monoclinic Friedel's salt). The existence of the two polymorphs for chloro-carboaluminate samples, monoclinic and rhombohedral, returns to the known structure transition of Friedel's salt (from the rhombohedral HT-structure to the monoclinic LT-structure at a transition temperature $T_s \approx 35^\circ\text{C}$ ^{5,6}). It has been shown that carbonation of Friedel's salt leads to the decrease of T_s which is about -15°C for AFm-[Cl_{0.75}·(CO₃)_{0.125}]-25°C.^{20,30} The carbonate-dependence of T_s explains the rhombohedral symmetry observed for AFm-[Cl_{0.75}·(CO₃)_{0.125}]-25°C sample. For samples containing the two polymorphs, no structural transition has been observed down to -120°C .²⁰ SEM analyses did not allow the determination of different chemical compositions for the two simultaneously present polymorphs. The 50 measurements performed for each sample did not show any significant variation in the calculated chemical composition in Ca, Al, and Cl. In the same way, the refined chemical composition of the rhombohedral chloro-carboaluminate polymorph is also closely related to the sample nominal composition (see $x_{ref.}$ values in Table II), which was close to the targeted nominal composition (Table II). Then,

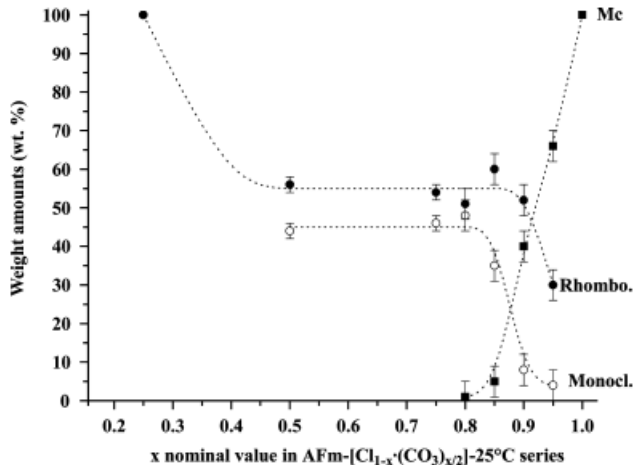


Fig. 3. Refined weight amounts of monocarboaluminate (Mc, full squares), rhombohedral polymorph (Rhomb., full circles), and monoclinic polymorph (Monocl., open circles) of chloro-carboaluminate phases in the AFm-[Cl_{1-x}·(CO₃)_{x/2}]-25°C series. Dotted lines are just guides for the eyes.

Table III. Lattice Parameters Refined by Rietveld Method for the Two Chloro-Carboaluminate Polymorphs Observed in Samples from Both AFm-[Cl_{1-x}·(CO₃)_{x/2}]-25°C and AFm-[Cl_{1-x}·(CO₃)_{x/2}]-85°C Series

| $x_{\text{nom.}}^{\dagger}$ | Rhombohedral polymorph | | | Monoclinic polymorph | | | | |
|--|------------------------|-------------|-----------------------|----------------------|------------|------------|-------------|-----------------------|
| | a (Å) | c (Å) | V (Å ³) | a (Å) | b (Å) | c (Å) | β (°) | V (Å ³) |
| <i>AFm-[Cl_{1-x}·(CO₃)_{x/2}]-25°C series</i> | | | | | | | | |
| 0.25 | 5.7465 (1) | 47.041 (1) | 1345.29 (4) | — | — | — | — | — |
| 0.50 | 5.7548 (1) | 46.9384 (9) | 1346.26 (4) | 10.0059 (8) | 5.7582 (5) | 16.231 (1) | 103.69 (2) | 908.6 (1) |
| 0.75 | 5.7643 (2) | 46.783 (1) | 1346.21 (8) | 9.9992 (5) | 5.7594 (3) | 16.350 (1) | 103.20 (1) | 916.7(1) |
| 0.80 | 5.7716 (3) | 46.888 (2) | 1349.5 (1) | 9.9931 (8) | 5.7588 (3) | 16.418 (2) | 103.78 (1) | 917.6 (1) |
| 0.85 | 5.7643 (1) | 46.889 (1) | 1349.28 (6) | 9.983 (1) | 5.759 (1) | 16.386 (2) | 103.05 (2) | 917.7 (3) |
| 0.90 | 5.7600 (1) | 46.809 (3) | 1344.98 (8) | 10.010 (1) | 5.755 (1) | 16.47 (1) | 104.6 (1) | 918 (1) |
| 0.95 | 5.7666 (3) | 46.782 (4) | 1347.2 (1) | 10.000 (1) | 5.758 (2) | 16.45 (2) | 104.1 (1) | 919 (2) |
| <i>AFm-[Cl_{1-x}·(CO₃)_{x/2}]-85°C series</i> | | | | | | | | |
| 0.25 | 5.7504 (1) | 46.9584 (9) | 1344.74 (4) | — | — | — | — | — |
| 0.50 | 5.7513 (1) | 46.9514 (7) | 1344.96 (4) | — | — | — | — | — |
| 0.75 | 5.7587 (1) | 46.8902 (9) | 1346.66 (4) | — | — | — | — | — |

[†] $x_{\text{nom.}}$ represents the x targeted nominal values of AFm-[Cl_{1-x}·(CO₃)_{x/2}] samples.

the presence of the two polymorphs could not be attributed to their chemical compositions.

(B) *Mineralogical Composition of Samples Belonging to the AFm-[Cl_{1-x}·(CO₃)_{x/2}]-85°C Series:* The samples synthesized at 85°C were single phased (Table II). For chloro-carboaluminate phase ($x = 0.25, 0.50,$ and 0.75), the rhombohedral structure was the only polymorph observed. Sample AFm-[(CO₃)_{0.500}]-85°C contained the triclinic monocarboaluminate phase only. The increase in the temperature of synthesis led to the stabilization of the rhombohedral polymorph: which exhibited the same symmetry than the Friedel's salt HT-structure. The single-phase feature of samples with $x = 0.25, 0.50,$ and 0.75 agrees with the existence of an AFm-[Cl⁻, CO₃²⁻] solid solution. Calculated chemical composition (from SEM analyses) and refined chemical composition (from Rietveld treatments) agreed fairly well with the targeted nominal composition (Table II). The previously supposed metastability feature of the monoclinic chloro-carboaluminate polymorph²⁰ is confirmed by its disappearance in the AFm-[Cl_{1-x}·(CO₃)_{x/2}]-85°C series. Structural parameters (lattice parameters) of rhombohedral polymorphs from both AFm-[Cl_{1-x}·(CO₃)_{x/2}]-25°C and AFm-[Cl_{1-x}·(CO₃)_{x/2}]-85°C series were comparable (Table III and Fig. 4): the red circles superimposed perfectly well with the black circles).

(C) *Variation of the Lattice Parameters for Both Chloro-Carboaluminate Polymorphs:* Refined lattice parameters of the two chloro-carboaluminate polymorphs are gathered in Table III, while the extracted variations of the interlayer distance d_0 ($d_0 = d_{006}$ and d_{002} for respectively the rhombohedral and the monoclinic polymorphs) and of the unit cell volume per motif V_0 ($V_0 = V/Z$ with $Z = 6$ and 4 for respectively the rhombohedral and the monoclinic polymorphs) are represented in Fig. 4 with the two series end-members: monocarboaluminate ($x = 1$) and Friedel's salt ($x = 0$, data taken from the literature⁴). The lattice parameters of the triclinic monocarboaluminate compound agreed well with the data taken from the literature¹ and remained invariant when observed in our samples ($a = 5.7763$ (5), respectively, 5.7797 (2) Å; $b = 8.4803$ (5), respectively, 8.4762 (2) Å; $c = 9.9393$ (6), respectively, 9.9285 (2) Å; $\alpha = 64.800$ (5), respectively, 64.709 (2)°; $\beta = 82.757$ (7), respectively, 82.795 (2)°; and $\gamma = 81.399$ (6), respectively, 81.401 (2)° for AFm-[(CO₃)_{0.500}]-25°C, respectively, AFm-[(CO₃)_{0.500}]-85°C samples). A great difference between the two chloro-carboaluminate polymorphs concerned the interlayer distance, which relates to the anionic organization into the interlayer region of the structure. The interlayer distance, as well as the unit cell volume (expressed per [Ca₂Al(OH)₆]·[X·nH₂O] motifs), increased from monocarboaluminate to the rhombohedral chloro-carboaluminate polymorph, and finally to the monoclinic chloro-carboaluminate polymorph. Another interesting observation was the great similitude between rhombohedral

phases synthesized at room temperature and at 85°C; variation of interlayer distances and of unit cell volumes with nominal composition superimposed fairly well. The temperature of synthesis of 85°C has stabilized the rhombohedral polymorph of chloro-carboaluminate without bringing any structural modifi-

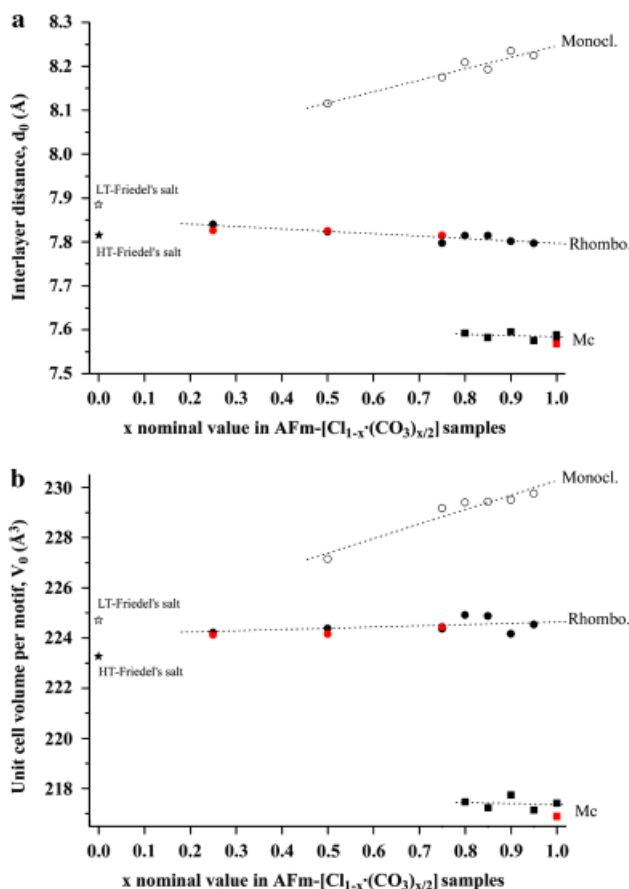


Fig. 4. Variations of the interlayer distance d_0 (a: d_{006} , d_{002} , and d_{011} for respectively the rhombohedral, monoclinic, and triclinic phases) and unit cell volume per motif V_0 [Ca₂Al(OH)₆]·[X·nH₂O] (b: $V/6$, $V/4$, and $V/2$ for respectively the rhombohedral, monoclinic, and triclinic phases) for samples belonging to both AFm-[Cl_{1-x}·(CO₃)_{x/2}]-25°C and AFm-[Cl_{1-x}·(CO₃)_{x/2}]-85°C series. Black symbols, respectively red symbols, correspond to the AFm-[Cl_{1-x}·(CO₃)_{x/2}]-25°C series, respectively AFm-[Cl_{1-x}·(CO₃)_{x/2}]-85°C. Mc, Rhombo, and Monoc. refer respectively to monocarboaluminate phase, rhombohedral polymorph and monoclinic polymorph of chloro-carboaluminate phase. Stars correspond to Friedel's salt values taken from Rapin *et al.*⁴ Dotted lines are linear fitting.

cation. Once again, this observation corroborated the metastability feature of the monoclinic chloro-carboaluminate polymorph.²⁰ The two sets of d_0 and V_0 values of Friedel's salt (i.e., LT- and HT-polymorphs reported in Fig. 4) were on both sides of the linear fitting relative to the rhombohedral chloro-carboaluminate polymorphs. However, taken into account that the difference between values from the two chloro-carboaluminate polymorphs decreased when the chloride content increased, it appears that the monoclinic LT-structure of Friedel's salt (that should be observed at room temperature), approximately lined with both chloro-carboaluminate polymorphs.

Accuracies of the refined lattice parameters of the two chloro-carboaluminate polymorphs suffered from peaks overlapping and widening. Nevertheless, the interlayer distance and unit cell volume of the monoclinic chloro-carboaluminate polymorph clearly increased with the carbonate amount in the $[\text{Ca}_2\text{Al}(\text{OH})_6] \cdot [\text{Cl}_{1-x} \cdot (\text{CO}_3)_{x/2} \cdot (2+x/2)\text{H}_2\text{O}]$ solid solution, whereas they were quite invariant in the rhombohedral chloro-carboaluminate polymorph case (Fig. 4). The interlayer distance increased greatly when going from monocarboaluminate to the rhombohedral chloro-carboaluminate polymorph. This increase can be explained by the location of carbonate anions: either directly bonded to the main layer in the monocarboaluminate structure,^{1,2} or at the center of the interlayer region in the rhombohedral chloro-carboaluminate structure.²⁰ The increase in the interlayer distance when going from the rhombohedral to the monoclinic chloro-carboaluminate polymorph was more surprising. It correlated with the increase observed during the structure transition of Friedel's salt (from the rhombohedral HT-structure to the monoclinic LT-structure), but to a greater extent (increase of about 0.35 Å, as compared with 0.12 Å for Friedel's salt) and the interlayer distance reached the value of about 8.2 Å for the monoclinic chloro-carboaluminate polymorph for x around 0.9. Such a large d_0 value is not compatible with a carbonate anion oriented parallel to main layer. The binitroaluminate AFm compound, in which nitrates are perpen-

dicular and bonded to main layer, has a d_0 value of 8.6 Å.^{7,8} The increase in the d_0 distance when increasing the carbonate amount in the monoclinic chloro-carboaluminate polymorph disagrees with conventional solid solution behavior. It could be explained by variable number of water in the interlayer space (not quantified in this work) and probably carbonate anions are not parallel to the main layer.

(2) Raman Spectroscopy

Raman spectroscopy was used to investigate the carbonate group environment within the interlayer region and the hydrogen bond network. Figure 5 reports the same parts of the spectra recorded for each sample in two spectral ranges: 200–1800 and 2800–3900 cm^{-1} .

Two bands of vibration were observed in the 200–1800 cm^{-1} spectral range (Figs. 5(a) and (c)): the $[\text{Al}(\text{OH})_6]$ vibration is around 530 cm^{-1} ,³¹ and the sample dependent A_{1g} vibration mode of carbonate group (symmetric stretching) around 1080 cm^{-1} . Spectra were systematically analyzed by using a line fitting procedure with a Lorentzian profile. Results, bands position and full-width at half maximum, are gathered in Table IV. The $[\text{Al}(\text{OH})_6]$ vibration, observed at a mean Raman shift of 532 cm^{-1} , did not depend on the x nominal value, or on the temperature of synthesis. Two clearly distinct positions were observed for the $[\text{CO}_3]$ symmetric stretching mode, which was x nominal value-dependent. The interpretation of these two positions is evidenced by the structure descriptions of monocarboaluminate^{1,2} and of the rhombohedral chloro-carboaluminate polymorph.²⁰ The $[\text{CO}_3]$ band at 1068 cm^{-1} is attributed to carbonate group directly bonded to the main layer (linked to Ca^{2+} cation), and the $[\text{CO}_3]$ band at 1086 cm^{-1} is attributed to the weakly bonded carbonate group located at the center of the interlayer. The evolution of the respective intensities of both carbonate bands agrees with the refined weight amounts of monocarboaluminate (with carbonate bonded to

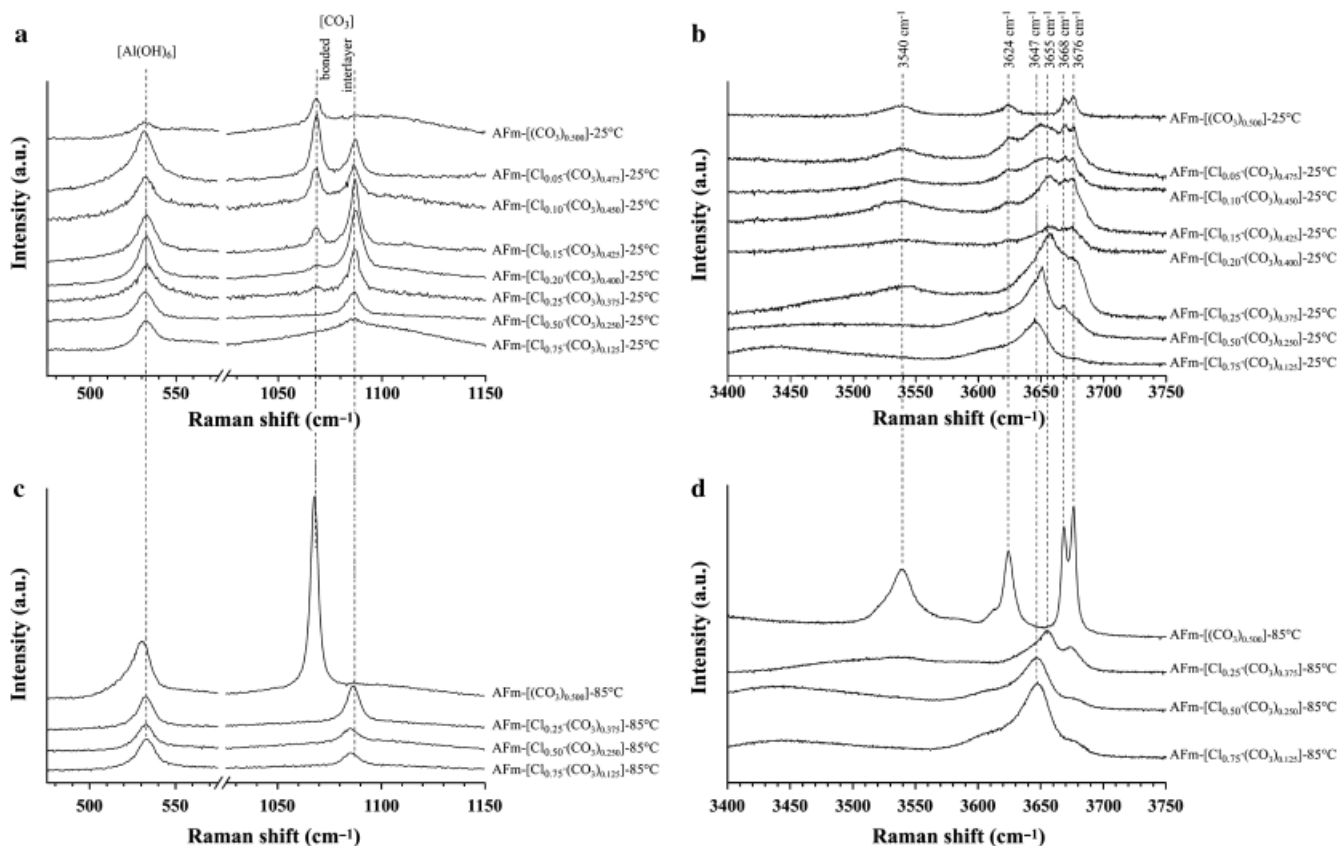


Fig. 5. Raman spectra from samples belonging to the AFm- $[\text{Cl}_{1-x} \cdot (\text{CO}_3)_{x/2}]$ -25°C series (a and b) and AFm- $[\text{Cl}_{1-x} \cdot (\text{CO}_3)_{x/2}]$ -85°C series (c and d) in the range spectra from 475 to 1150 cm^{-1} (a and c: $[\text{Al}(\text{OH})_6]$ and $[\text{CO}_3]$ symmetric stretching) and from 3400 to 3750 cm^{-1} (b and d: O–H stretching).

Table IV. Symmetric Stretching of Carbonate in Raman Spectra from Both Chloro-Carboaluminate Series

| $x_{\text{nom.}}^{\dagger}$ | [Al(OH) ₆] | | [CO ₃] | | | |
|--|---------------------------------|--------------------------|---------------------------------|--------------------------|---------------------------------|--------------------------|
| | Raman shift (cm ⁻¹) | FWHM (cm ⁻¹) | Bonded to main layer | | Interlayer | |
| | | | Raman shift (cm ⁻¹) | FWHM (cm ⁻¹) | Raman shift (cm ⁻¹) | FWHM (cm ⁻¹) |
| <i>AFm-[Cl_{1-x}·(CO₃)_{x/2}]-25°C series</i> | | | | | | |
| 0.25 | 532.4 | 10.0 | — | — | 1086.3 | 5.8 |
| 0.50 | 531.7 | 10.1 | — | — | 1086.2 | 6.6 |
| 0.75 | 532.5 | 9.2 | 1068.4 | 5.1 | 1087.3 | 5.8 |
| 0.80 | 532.3 | 8.8 | 1067.7 | 5.0 | 1086.8 | 5.5 |
| 0.85 | 532.7 | 8.7 | 1068.2 | 4.3 | 1087.0 | 4.3 |
| 0.90 | 532.2 | 8.9 | 1067.9 | 4.7 | 1086.6 | 4.5 |
| 0.95 | 532.9 | 9.2 | 1068.3 | 4.1 | 1087.1 | 4.5 |
| 1.00 | 531.7 | 9.3 | 1068.3 | 4.0 | — | — |
| <i>AFm-[Cl_{1-x}·(CO₃)_{x/2}]-85°C series</i> | | | | | | |
| 0.25 | 533.1 | 10.3 | — | — | 1085.6 | 7.3 |
| 0.50 | 532.7 | 9.5 | — | — | 1085.1 | 7.7 |
| 0.75 | 532.8 | 8.8 | — | — | 1086.5 | 6.3 |
| 1.00 | 530.9 | 10.1 | 1067.9 | 4.3 | — | — |

[†] $x_{\text{nom.}}$ represents the x targeted nominal values of AFm-[Cl_{1-x}·(CO₃)_{x/2}] samples. FWHM, full-width at half maximum.

main layer; i.e., the signal at 1068 cm⁻¹) and of both chloro-carboaluminate polymorphs (with carbonate located in the interlayer; i.e., the signal at 1086 cm⁻¹). We were not able to differentiate the monoclinic and the rhombohedral chloro-carboaluminate polymorphs (neither by the band position nor by the band width). This agrees with the previously described carbonate anion position in the monoclinic polymorph in section 3.1, located at the center of interlayer, more or less parallel to the main layer (in a similar way with the rhombohedral polymorph). Attribution of the two [CO₃] stretching signals stands for both AFm-[Cl_{1-x}·(CO₃)_{x/2}]-25°C and AFm-[Cl_{1-x}·(CO₃)_{x/2}]-85°C series. The presence of monocarboaluminate was observed down to the x value of 0.75 (AFm-[Cl_{0.25}·(CO₃)_{0.375}]-25°C sample with an extremely weak band of vibration at 1068 cm⁻¹) illustrating the high sensitivity of Raman spectroscopy.

The spectral range 2800–3900cm⁻¹ (Figs. 5(b) and (d)) gave an image of the hydrogen bond network. The ordered structure of monocarboaluminate¹ led to a perfectly described interlayer region with finite hydrogen bonds (in number and in interatomic distances). This correlates with the well-defined O–H elongations for AFm-[(CO₃)_{0.500}]-85°C samples and also AFm-[(CO₃)_{0.500}]-25°C sample: bands of vibrations resolved and centered at 3540, 3624, 3668, and 3676 cm⁻¹. The Raman spectra of other AFm phases do not show such resolved O–H bands of vibrations: both monosulfoaluminate³¹ and binitroaluminate⁸ present a dynamical disorder of the anionic species, characteristic of a disorder in the interlayer part of the structure. When chloride anions were substituted by carbonate anions (i.e., when decreasing the x nominal value), the resolved O–H bands of vibrations were gradually replaced by a broader signal. For $x = 0.75$ samples (both AFm-[Cl_{0.25}·(CO₃)_{0.375}]-25°C and AFm-[Cl_{0.25}·(CO₃)_{0.375}]-85°C), two broad bands are observed at 3665 and 3670 cm⁻¹. This unresolved signal was displaced to 3647 cm⁻¹ in $x = 0.25$ samples (both AFm-[Cl_{0.75}·(CO₃)_{0.125}]-25°C and AFm-[Cl_{0.75}·(CO₃)_{0.125}]-85°C samples): spectra recorded from the two AFm-[Cl_{1-x}·(CO₃)_{x/2}]-25°C and AFm-[Cl_{1-x}·(CO₃)_{x/2}]-85°C series showed the same evolution when increasing the x value, indicating that the two chloro-carboaluminate polymorphs were not distinguishable by the Raman signature of their hydrogen bond networks.

(3) ²⁷Al MAS NMR

²⁷Al MAS NMR spectroscopy was used to investigate, and discriminate if possible, the mixed AFm phases. The first sphere of coordination of aluminum atoms is unmodified (or weakly modified) in the different AFm phases with six hydroxyl anions, but the second sphere of coordination is highly dependent on the

interlayer anions. ²⁷Al MAS NMR spectra are presented in Fig. 6 for all the synthesized samples. All spectra showed signals entirely assignable to Al in octahedral coordination (with peaks maxima near 5–10 ppm). Nevertheless, spectra from AFm-[(CO₃)_{0.500}]-25°C and AFm-[(CO₃)_{0.500}]-85°C samples differed significantly from the others. Both presented a broader signal, and shifted toward the lower chemical shift values. The distinct behavior of the monocarboaluminate samples was attributed to the direct bonding of carbonate anion to main layer. The profile line analyses of the spectra from AFm-[(CO₃)_{0.500}]-25°C and AFm-[(CO₃)_{0.500}]-85°C samples could be decomposed into two distinct resonances (close to 4.5 and 7 ppm), attributed to the triclinic AFm phase (see Table V), in agreement with its structural description, which includes two distinct aluminum crystallographic sites (for both ordered $P1^1$ and disordered $P1^2$ modifications). Resonances centered at around 1 ppm, respectively, 12.5 ppm, were attributed to impurities: AH₃,^{30,31} respectively C₃AH₆.³⁰ Spectra recorded from the AFm-[Cl_{1-x}·(CO₃)_{x/2}]-85°C series with $x < 1.00$ were composed of a single resonance for the AFm phase, with a peak maximum near 8.5 ppm. The position of this peak maximum was weakly shifted toward smaller chemical shift values when increasing the chloride amount (8.7, 8.1, and 8.0 ppm respectively for AFm-[Cl_{0.25}·(CO₃)_{0.375}]-85°C, AFm-[Cl_{0.50}·(CO₃)_{0.250}]-85°C, and AFm-[Cl_{0.75}·(CO₃)_{0.125}]-85°C, respectively). The single-phase $x = 0.25$ sample from the AFm-[Cl_{1-x}·(CO₃)_{x/2}]-25°C series, also presented a single resonance at 7.7 ppm. The other spectra from samples belonging to the AFm-[Cl_{1-x}·(CO₃)_{x/2}]-25°C series (0.5 ≤ x ≤ 0.95) were decomposed by considering two (quite unresolved) resonances: one near 8.5 ppm and the other near 6 ppm. According to these observations on both series, we could attribute the resonance near 8.5 ppm to the rhombohedral chloro-carboaluminate polymorph. The peak maximum of this resonance increased (from 8 to 9 ppm) when decreasing the chloride amount (i.e., increasing the carbonate substitution). The resonance near 6 ppm (observed between 5.3 and 7.5 ppm) was then attributed to the monoclinic chloro-carboaluminate polymorph. The weak difference between the resonance maxima of the two chloro-carboaluminate polymorphs has to be interpreted by their large similarity concerning the aluminum environment.

IV. Discussion

Three simultaneously present AFm phases can be observed in the AFm-[Cl_{1-x}·(CO₃)_{x/2}]-25°C series: monocarboaluminate and two chloro-carboaluminate polymorphs (i.e., two kinds of Cl⁻-CO₃²⁻ permutation; one described in the rhombohedral

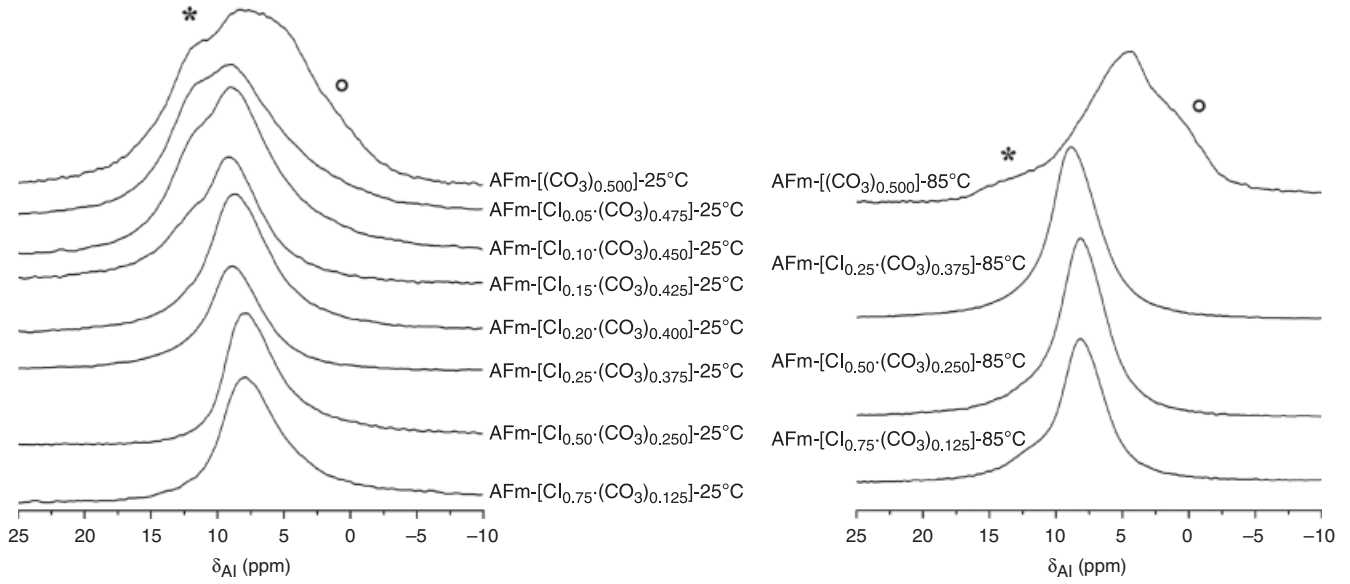


Fig. 6. ^{27}Al MAS NMR spectra from both AFm-[$\text{Cl}_{1-x} \cdot (\text{CO}_3)_{x/2}$]-25°C series (left) and AFm-[$\text{Cl}_{1-x} \cdot (\text{CO}_3)_{x/2}$]-85°C series (right). Marks * and \circ respectively correspond to signals from katoite (C_3AH_6) and $\text{Al}(\text{OH})_3$.

symmetry, and the other described in the monoclinic symmetry). The crystallographic structure of the rhombohedral polymorph has been recently characterized by single-crystal XRD experiment.²⁰ The newly observed monoclinic chloro-carboaluminate polymorph is metastable, as indicated by its systematic absence in the AFm-[$\text{Cl}_{1-x} \cdot (\text{CO}_3)_{x/2}$]-85°C series. All the samples from this series are single phased and composed only of monocarboaluminate ($x = 1$) or of rhombohedral chloro-carboaluminate polymorph ($x = 0.75, 0.50, \text{ and } 0.25$). The existence of the two monoclinic and rhombohedral polymorphs for the $\text{Cl}^- - \text{CO}_3^{2-}$ permuted AFm phase refers to the known Friedel's salt structure transition.^{4,5,30} The temperature of transition, T_s , is about 35°C for pure Friedel's salt and quickly decreases when carbonate substitutes for chloride (T_s

is about -15°C for AFm-[$\text{Cl}_{0.75} \cdot (\text{CO}_3)_{0.125}$]-25°C).²⁰ This dependence of T_s versus the carbonate substitution indicates that the rhombohedral polymorph of chloro-carboaluminate should only be observed, and reinforces the assumed metastable feature of the monoclinic polymorph in the AFm-[$\text{Cl}_{1-x} \cdot (\text{CO}_3)_{x/2}$]-25°C series. The metastable monoclinic polymorph appears when a sufficient carbonate to chloride permutation is reached (i.e., for $x \geq 0.5$ in the AFm-[$\text{Cl}_{1-x} \cdot (\text{CO}_3)_{x/2}$]-25°C series), and is replaced by monocarboaluminate at large carbonate amount (i.e., at $x > 0.85$ in the AFm-[$\text{Cl}_{1-x} \cdot (\text{CO}_3)_{x/2}$]-25°C series). The domain of existence of the rhombohedral stable polymorph is more extended: it is already observed at $x = 0.25$ (and exists certainly for $x < 0.25$) and up to $x = 0.95$. Then, the presence of the two chloro-carboaluminate polymorphs in the samples

Table V. Result of the Profile Fitting Analyses of the ^{27}Al MAS NMR Spectra from Both Chloro-Carboaluminate Series

| $x_{\text{nom.}}^\ddagger$ | AFm-[$\text{Cl}_{1-x} \cdot (\text{CO}_3)_{x/2}$]-25°C series | | | AFm-[$\text{Cl}_{1-x} \cdot (\text{CO}_3)_{x/2}$]-85°C series | | |
|----------------------------|---|------------|-----------------------|---|------------|-----------------------|
| | δ_{Al} (ppm) | FWHM (ppm) | Pop. [‡] (%) | δ_{Al} (ppm) | FWHM (ppm) | Pop. [‡] (%) |
| 0.25 | 1.2 ^a | 8.1 | 12 | 8.0 | 3.7 | 95 |
| | 7.7 | 4.4 | 88 | 12.4 ^b | 3.0 | 5 |
| | 5.4 | 5.7 | 47 | 8.1 | 3.8 | 96 |
| 0.5 | 8.0 | 3.1 | 53 | 12.8 ^b | 4.1 | 4 |
| | 6.4 | 5.0 | 35 | 8.7 | 4.0 | 100 |
| 0.75 | 8.9 | 4.5 | 65 | — | — | — |
| | 7.5 | 6.2 | 46 | — | — | — |
| | 9.0 | 4.0 | 54 | — | — | — |
| 0.85 | 7.5 | 4.3 | 20 | — | — | — |
| | 9.1 | 5.0 | 70 | — | — | — |
| | 12.8 ^b | 4.0 | 10 | — | — | — |
| 0.90 | 5.3 | 8.8 | 24 | — | — | — |
| | 8.9 | 5.3 | 67 | — | — | — |
| | 12.3 ^b | 2.9 | 9 | — | — | — |
| 0.95 | 5.4 | 9.1 | 36 | — | — | — |
| | 8.8 | 5.8 | 54 | — | — | — |
| | 12.5 ^b | 3.1 | 10 | — | — | — |
| 1.00 | 1.1 ^a | 3.3 | 4 | 0.7 ^a | 3.0 | 10 |
| | 4.5 | 4.8 | 34 | 4.2 | 4.5 | 45 |
| | 7.9 | 4.5 | 53 | 6.7 | 5.8 | 42 |
| | 12.3 ^b | 4.2 | 9 | 12.8 ^b | 4.0 | 2 |

[‡] $x_{\text{nom.}}$ represents the x targeted nominal values of AFm-[$\text{Cl}_{1-x} \cdot (\text{CO}_3)_{x/2}$] samples. [‡]Relative populations of the signals obtained by profile fitting (normalized to 100% of aluminum atoms). a and b signals attributed respectively to AH_3 and C_3AH_6 impurities. FWHM, full-width at half maximum; Pop., population.

complicates the interpretation in terms of $[\text{Ca}_2\text{Al}(\text{OH})_6] \cdot [\text{Cl}_{1-x} \cdot (\text{CO}_3)_{x/2} \cdot (2+x/2)\text{H}_2\text{O}]$ solid solution, but the results agree with its existence in a large range, namely considering the stable rhombohedral polymorph. The two-end members, the triclinic monocarboaluminate and the monoclinic Friedel's salt, should not belong to this solid solution due to symmetry considerations. According to our results, the rhombohedral $[\text{Ca}_2\text{Al}(\text{OH})_6] \cdot [\text{Cl}_{1-x} \cdot (\text{CO}_3)_{x/2} \cdot (2+x/2)\text{H}_2\text{O}]$ solid solution exists for $0.25 \leq x \leq 0.95$. However, supplementary syntheses in the chloride-rich side are needed to accurately determine the x lower limit. The x dependence of the lattice of the monoclinic chloro-carboaluminate polymorph also agrees with the existence of a monoclinic $[\text{Ca}_2\text{Al}(\text{OH})_6] \cdot [\text{Cl}_{1-x} \cdot (\text{CO}_3)_{x/2} \cdot (2+x/2)\text{H}_2\text{O}]$ solid solution in a less extended domain with $0.50 \leq x \leq 0.90$. The large interlayer distance observed for the monoclinic chloro-carboaluminate polymorph indicates that carbonate anions are located in the interlayer region more or less parallel to the main layer, in a manner similar to the carbonate location in the rhombohedral polymorph.²⁰ Raman spectra have confirmed the equivalent anionic arrangement in both chloro-carboaluminate polymorphs with a $[\text{CO}_3]$ stretching band at 1086 cm^{-1} characteristic of interlayer carbonate (whereas carbonate directly bonded to main layer in monocarboaluminate is characterized by a stretching band at 1068 cm^{-1}).²⁷ Al MAS NMR spectroscopy has indicated a similar Al environment in the two chloro-carboaluminate polymorphs. Indeed, the resonance maxima are found to be close between the monoclinic polymorph (6 ppm) and the rhombohedral polymorph (8.5 ppm).

V. Conclusion

Twelve AFm- $[\text{Cl}_{1-x} \cdot (\text{CO}_3)_{x/2}]$ samples were synthesized at two temperature (25° and 85°C) and studied in detail by Rietveld treatments of PXRD patterns, SEM analyses, Raman spectroscopy, and ²⁷Al NMR spectroscopy in order to combine long-range order characterization with local environment description. Existence of solid solution $[\text{Ca}_2\text{Al}(\text{OH})_6] \cdot [\text{Cl}_{1-x} \cdot (\text{CO}_3)_{x/2} \cdot (2+x/2)\text{H}_2\text{O}]$ in AFm phases, due to chloride to carbonate permutation, was investigated and described in detail. This solid solution, with $0.25 \leq x \leq 0.95$ according to our samples, had a stable rhombohedral symmetry, in agreement with the recent crystallographic description of the chloro-carboaluminate compound of composition $[\text{Ca}_2\text{Al}(\text{OH})_6] \cdot [\text{Cl}_{0.5} \cdot (\text{CO}_3)_{0.25} \cdot 2.25 \text{H}_2\text{O}]$.²⁰ Samples synthesized at room temperature also contained a metastable monoclinic polymorph of the $[\text{Ca}_2\text{Al}(\text{OH})_6] \cdot [\text{Cl}_{1-x} \cdot (\text{CO}_3)_{x/2} \cdot (2+x/2)\text{H}_2\text{O}]$ solid solution. The structure relationship between the stable rhombohedral and metastable monoclinic polymorphs corresponds to the one observed between the rhombohedral HT- and the monoclinic LT-Friedel's salt structures. Raman spectroscopy was particularly useful to locate carbonate anions into the structure with two distinct signals for carbonate bonded to main layer (symmetric stretching at 1068 cm^{-1} , monocarboaluminate case) and carbonate located at the center of the interlayer region (symmetric stretching at 1068 cm^{-1} , chloro-carboaluminate case).²⁷ Al MAS NMR spectroscopy highlighted the weak structural differences between the two chloro-carboaluminate polymorphs (which present weakly different aluminum environments).

Acknowledgment

Laurent Petit, from Electricité de France, is deeply acknowledged for his support on this study.

References

1. M. François, G. Renaudin, and O. Evrard, "A Cementitious Compound with Composition $3\text{CaO} \cdot \text{Al}_2\text{O}_3 \cdot \text{CaCO}_3 \cdot 11\text{H}_2\text{O}$," *Acta Crystallogr. Sec. C: Cryst. Struct. Commun.*, **54** [9] 1214–7 (1998).
2. G. Renaudin, M. François, and O. Evrard, "Order and Disorder in the Lamellar Hydrated Tetracalcium Monocarboaluminate Compound," *Cem. Concr. Res.*, **29** [1] 63–9 (1999).

3. R. Allmann, "Refinement of the Hybrid Layer Structure Hexahydroxaluminocalcium Hemisulfate Trihydrate $[\text{Ca}_2\text{Al}(\text{OH})_6] [1/2\text{SO}_4 \cdot 3\text{H}_2\text{O}]$," *Neues Jahrb. Mineral. Monatsh.*, 136–44, (1977).

4. J. P. Rapin, G. Renaudin, E. Elkaim, and M. François, "Structural Transition of Friedel's Salt $3\text{CaO} \cdot \text{Al}_2\text{O}_3 \cdot \text{CaCl}_2 \cdot 10\text{H}_2\text{O}$ Studied by Synchrotron Powder Diffraction," *Cem. Concr. Res.*, **32** [4] 513–9 (2002).

5. G. Renaudin, F. Kubel, J. P. Rivera, and M. François, "Structural Phase Transition and High Temperature Phase Structure of Friedel's Salt, $3\text{CaO} \cdot \text{Al}_2\text{O}_3 \cdot \text{CaCl}_2 \cdot 10\text{H}_2\text{O}$," *Cem. Concr. Res.*, **29** [12] 1937–42 (1999).

6. A. Terzis, S. Filippakis, H.-J. Kuzel, and H. Bruzlaiff, "The Crystal Structure of $\text{Ca}_2\text{Al}(\text{OH})_6\text{Cl} \cdot 2\text{H}_2\text{O}$," *Zeitschr. Kristallogr.*, **181** [1–4] 29–34 (1987).

7. G. Renaudin and M. François, "The Lamellar Double-Hydroxide (LDH) Compound with Composition $3\text{CaO} \cdot \text{Al}_2\text{O}_3 \cdot \text{Ca}(\text{NO}_3)_2 \cdot 10\text{H}_2\text{O}$," *Acta Crystallogr. Sec. C: Cryst. Struct. Commun.*, **55** [6] 835–8 (1999).

8. G. Renaudin, J. P. Rapin, B. Humbert, and M. François, "Thermal Behaviour of the Nitrated AFm Phase $\text{Ca}_4\text{Al}_2(\text{OH})_{12}(\text{NO}_3)_2 \cdot 4\text{H}_2\text{O}$ and Structure Determination of the Intermediate Hydrate $\text{Ca}_4\text{Al}_2(\text{OH})_{12}(\text{NO}_3)_2 \cdot 2\text{H}_2\text{O}$," *Cem. Concr. Res.*, **30** [2] 307–14 (2000).

9. G. Renaudin, J. P. Rapin, E. Elkaim, and M. François, "Polytypes and Polymorphs in the Related Friedel's Salt $[\text{Ca}_2\text{Al}(\text{OH})_6]^{+} [\text{X} \cdot 2\text{H}_2\text{O}]^{-}$ Halide Series," *Cem. Concr. Res.*, **34** [10] 1845–52 (2004).

10. A. Walcarius, G. Lefevre, J. P. Rapin, G. Renaudin, and M. François, "Voltammetric Detection of Iodide After Accumulation by Friedel's Salt," *Electroanalysis*, **13** [4] 313–20 (2001).

11. J. P. Rapin, A. Walcarius, G. Lefevre, and M. François, "A Double-Layered Hydroxide, $3\text{CaO} \cdot \text{Al}_2\text{O}_3 \cdot \text{CaI}_2 \cdot 10\text{H}_2\text{O}$," *Acta Crystallogr. Sec. C: Cryst. Struct. Commun.*, **55** [12] 1957–9 (1999).

12. R. Segni, N. Allali, L. Vieille, C. Taviot-Guého, and F. Leroux, "Hydrocalumite-Type Materials: 2. Local Order into $\text{Ca}_2\text{Fe}(\text{OH})_6(\text{CrO}_4)_{0.5} \cdot n\text{H}_2\text{O}$ in Temperature Studied by X-Ray Absorption and Mössbauer Spectroscopies," *J. Phys. Chem. Solids*, **67** [5–6] 1043–7 (2006).

13. R. Segni, L. Vieille, F. Leroux, and C. Taviot-Guého, "Hydrocalumite-Type Materials: 1. Interest in Hazardous Waste Immobilization," *J. Phys. Chem. Solids*, **67** [5–6] 1037–42 (2006).

14. M. Balonis and F. P. Glasser, "The Density of Cement Phases," *Cem. Concr. Res.*, **39** [9] 733–9 (2009).

15. F. P. Glasser, A. Kindness, and S. A. Stronach, "Stability and Solubility Relationships in AFm Phases: Part I. Chloride, Sulfate and Hydroxide," *Cem. Concr. Res.*, **29** [6] 861–6 (1999).

16. T. Matschei, B. Lothenbach, and F. P. Glasser, "The AFm Phase in Portland Cement," *Cem. Concr. Res.*, **37** [2] 118–30 (2007).

17. U. A. Birnin-Yauri and F. P. Glasser, "Friedel's Salt, $\text{Ca}_2\text{Al}(\text{OH})_6(\text{Cl},\text{OH}) \cdot 2\text{H}_2\text{O}$: Its Solid Solutions and their Role in Chloride Binding," *Cem. Concr. Res.*, **28** [12] 1713–23 (1998).

18. H. Hirao, K. Yamada, H. Takahashi, and H. Zibara, "Chloride Binding of Cement Estimated by Binding Isotherms of Hydrates," *J. Adv. Concr. Technol.*, **3** [1] 77–84 (2005).

19. M. Sacerdoti and E. Passaglia, "Hydrocalumite from Latium, Italy: Its Crystal Structure and Relationship with Related Synthetic Phases," *Neues Jahrb. Mineral. Monatsh.*, **10**, 462–75 (1988).

20. A. Mesbah, J.-P. Rapin, M. François, C. Cau-dit-Coumes, F. Frizon, F. Leroux, and G. Renaudin, "Crystal Structures and Phase Transition of Cementitious Bi-Anionic AFm- $(\text{Cl}^-, \text{CO}_3^{2-})$ Compounds," *J. Am. Ceram. Soc.*, **94** [1] 261–8 (2011).

21. M. Balonis, B. Lothenbach, G. Le Saout, and F. P. Glasser, "Impact of Chloride on the Mineralogy of Hydrated Portland Cement Systems," *Cem. Concr. Res.*, **40** [7] 1009–22 (2010).

22. H. Pöllmann, "Mischkristallbildung in den systemen $3\text{CaO} \cdot \text{Al}_2\text{O}_3 \cdot \text{CaCl}_2 \cdot 10\text{H}_2\text{O}$ – $3\text{CaO} \cdot \text{Al}_2\text{O}_3 \cdot \text{CaCO}_3 \cdot 11\text{H}_2\text{O}$ – $3\text{CaO} \cdot \text{Al}_2\text{O}_3 \cdot \text{Ca}(\text{OH})_2 \cdot 12\text{H}_2\text{O}$," Ph.D. Thesis, Erlangen, Germany, 1984.

23. M. Hobbs, "Solubilities And Ion Exchange Properties Of Solid Solutions between The OH, Cl, CO_3 End Members of the Monocalcium Aluminate Hydrates," Ph.D. Thesis, University of Waterloo, 2001.

24. L. W. Finger, D. E. Cox, and A. P. Jephcoat, "Correction for Powder Diffraction Peak Asymmetry Due to Axial Divergence," *J. Appl. Crystallogr.*, **27** [Part 6] 892–900 (1994).

25. J. Rodriguez-Carvajal, "Recent Advances in Magnetic Structure Determination by Neutron Powder Diffraction," *Phys. B: Condens. Matter*, **192** [1–2] 55–69 (1993).

26. M. D. Andersen, H. J. Jakobsen, and J. Skibsted, "A new Aluminium-Hydrate Species in Hydrated Portland Cements Characterized by ²⁷Al and ²⁹Si MAS NMR Spectroscopy," *Cem. Concr. Res.*, **36** [1] 3–17 (2006).

27. P. Faucon, T. Charpentier, D. Bertrandie, A. Nonat, J. Virllet, and J. C. Petit, "Characterization of Calcium Aluminate Hydrates and Related Hydrates of Cement Pastes by ²⁷Al MQ-MAS NMR," *Inorg. Chem.*, **37** [15] 3726–33 (1998).

28. P. Faucon, A. Delagrave, J. C. Petit, C. Richet, J. M. Marchand, and H. Zanni, "Aluminum Incorporation in Calcium Silicate Hydrates (C–S–H) Depending on Their Ca/Si Ratio," *J. Phys. Chem. B*, **103** [37] 7796–802 (1999).

29. G. K. Sun, J. F. Young, and R. J. Kirkpatrick, "The Role of Al in C–S–H: NMR, XRD, and Compositional Results for Precipitated Samples," *Cem. Concr. Res.*, **36** [1] 18–29 (2006).

30. R. J. Kirkpatrick, P. Yu, X. Hou, and Y. Kim, "Interlayer Structure, Anion Dynamics, and Phase Transitions in Mixed-Metal Layered Hydroxides: Variable Temperature ³⁵Cl NMR Spectroscopy of Hydrotalcite and Ca-Aluminate Hydrate (Hydrocalumite)," *Am. Mineral.*, **84** [7–8] 1186–90 (1999).

31. G. Renaudin, R. Segni, D. Mentel, J.-M. Nedelec, F. Leroux, and C. Taviot-Guého, "A Raman Study Oh the Sulfated Cement Hydrates: Ettringite and Monosulfoaluminate," *J. Adv. Concr. Technol.*, **5** [3] 299–312 (2007). □